Technical Note PR-TN 2010/00487

Issued: 11/2010

Simulations on 3D shape tracking with fibre Bragg gratings

G.W. 't Hooft; A. Tirard-Gâtel

Philips Research Europe

Authors' address

G.W. 't Hooft	HTC34-21	gert.hooft@philips.com
A. Tirard-Gâtel		arnaud.tirardgatel@gmail.com

Title:	Simulations on 3D shape tracking with fibre Bragg gratings
Author(s):	G.W. 't Hooft; A. Tirard-Gâtel
Reviewer(s):	Busch, H. von, Chan, R., IPS Facilities, Manzke, R.
Technical Note:	PR-TN 2010/00487
Additional Numbers:	
Subcategory:	
Project:	Smart Delivery System (2009-229)
Customer:	

Keywords: Bragg gratings, fibre optic sensors, 3D reconstruction, 3D tracking

Abstract: This report deals with the development of a reconstruction algorithm of 3D optical shape sensing. The theoretical frame work is established and simulations are performed for a multicore fiber system without torque.

Conclusions: The modelling of the Bragg sensors to reconstruct the geometry of a multicore fiber has been accomplished with good results. The relative errors are in the order of 0.001% for a fiber bended as a standard helix and 0.02% for an expanding helix. The influence of noise in the reflection spectra is simulated. The error in the reconstruction increases up to 0.1% (factor of 100 compared to the case without noise) for a noise level of only 0.5% in magnitude. This sets a standard for the accuracy of experimental data.

Management Summary

The purpose of the project, called Smart Delivery System, is to develop medical instruments that can be tracked by optical interrogation methods. In these medical devices optical fibers are embedded. These fibers contain Bragg gratings that act as strain sensors. The amount of strain can be monitored by measuring the reflection spectrum with an interferometric method. In this report the theory is given how form of the fiber influences strain and consequentually the reflection spectrum. Subsequently, the reverse process is established, by formulating an algorithm that analyses the reflection spectrum of multicore fibers containing Bragg gratings leading to the reconstruction of the 3D shape. The accuracy of the algorithm scales quadratically with the number of points, and is inversely proportional with square of the torsion, i.e. the 3 dimensional nature of the shape. For a helical structure of 1 m length the algorithm gives an accuracy of 10 μm using a 150 μm step size, while the fiber contains 3 cores each having 39 Bragg gratings of 25 mm nominal length and a nominal separation of 1 mm. This algorithm is more than adequate for minimally invasive medical procedures where accuracies in the mm range are needed. The influence of amplitude noise, more complicated structures such as an expanding helix, and registration errors between the various cores of the multicore fiber are also reported in this technical note. In future work the influence of torque, strain induced birefringence and laser noise characteristics should be investigated.

Contents

1. Introduction

One of the techniques to track an elongated medical device is fiber optic shape sensing. In the medical device, such as a catheter, guide wire or endoscope, an optical fiber with multiple cores is embedded. Light is sent through the optical fiber and the spectrum of the reflected light from each of the cores is separately detected with a phase sensitive method. Any curvature of the fiber will induce strain in the fiber cores and consequently the spectrum will alter. The shape sensing technique constitutes, therefore, of the following steps: Firstly, a measurement of the spectrum of the reflected light. Secondly, the strain as a function of position along the fiber is calculated. Thirdly, reconstruction of the shape of the fiber in 3 dimensional space using curvature values deduced from the strain.

1.1. Objective

The objective of this document is to elucidate a reliable method for steps two and three, i.e. establish an algorithm to calculate the strain as function of position from reflection as a function of wavelength, and from strain to calculate the curvature and from curvature the shape. In this document we will take the measurement technique and method for granted. In fact we will not use experimental data but synthetically generated spectra from a forward calculation. In doing so we can concentrate on the reliability of the algorithm without being hampered by noise inherently present in experimental data. The robustness of the algorithm can be tested by adding artificial noise.

1.2. Approach and outline of the technical note

As the title of this technical note suggest we will be working with the reflection spectra from fiber Bragg gratings. We will start in chapter 2 by describing what a fiber Bragg grating is and what the characteristics of its reflection spectrum are. In what follows, we will adhere ourselves to the small signal approximation, i.e. the cases where the reflection amplitudes are small, and explain why this is a convenient regime. Then we will describe the sensitivity to strain and temperature. From this it is straightforward to expand to multiple distributed Bragg gratings along the core of a fiber and in doing so establish a forward calculation. In chapter 3 the reverse procedure is followed, i.e. from the reflection spectra of the various cores in the fiber the strain as a function of position is calculated. Subsequently, a recursive algorithm is formulated with which the distributed strain can be transferred into shape. The accuracy of this method will be evaluated using two example shapes, viz. a standard helix and a helix with a linearly increasing radius. In the appendices background information can be found such as the derivation of the coupled wave equations describing the transmission and reflection of Bragg gratings, the exact solution of these coupled differential equations for a homogeneous grating, and the Fourier relationship between the reflectivity and the taper function for the case of small wave coupling.

1.3. Intended audience

Who should read this masterpiece? Apart from those that have nothing better to do, those that are interested in the fundamentals of fiber Bragg gratings, those that would like to know the principles and limitations of fiber optic shape sensing and localization, those who think they have a superior shape reconstruction method and would like to calibrate, and any combination of these categories.

2. Reflection spectrum of Fiber Bragg gratings

Consider a single mode optical fiber with a refractive index n_{co} of the core which is slightly larger than the refractive index n_{cl} of the cladding. Imagine that the refractive index of the core is not constant but exhibits a periodically modulation in the longitudinal direction of the fiber. The modulation acts as a grating with a wave vector $G = 2\pi/\Lambda$, where Λ is the periodicity of the modulation. When the wave vector of the light $2\pi n/\lambda$ propagating in the fundamental mode of the fiber equals half the one of the grating a resonance occurs in the reflection. This is the Bragg condition:

$$\lambda_b = 2n\Lambda \tag{2.1}$$

For light in the telecommunication regime around 1500 nm and a refractive index of the mode of 1.5 the Bragg resonance occurs for modulations with periods around 500 nm. Usually, they are manufactured by illumination of Ge doped fibers with UV light using holograms or other interferometric methods. The magnitude of the Bragg resonance is determined by an effective mode coupling constant Ω, which is an average of the dielectric constant variation over the mode profile. Its formula is derived in the appendix (A1.14). The mode coupling constant has the dimension of an inverse length and can be viewed as a gain/loss coefficient, i.e. the length of fiber over which the light has to travel at the Bragg resonance in order for the amplitude to decrease by 1/e, while at the same time the counter propagating wave is increasing by a similar factor or vice versa. The Fresnel reflection coefficient at resonance scales with the product of mode coupling constant Ω and grating length L, so that the intensity reflection coefficient scales with the square of this product. In appendix A2 the exact formula for the reflection spectrum is derived for the case of a grating with constant periodicity and constant mode coupling.

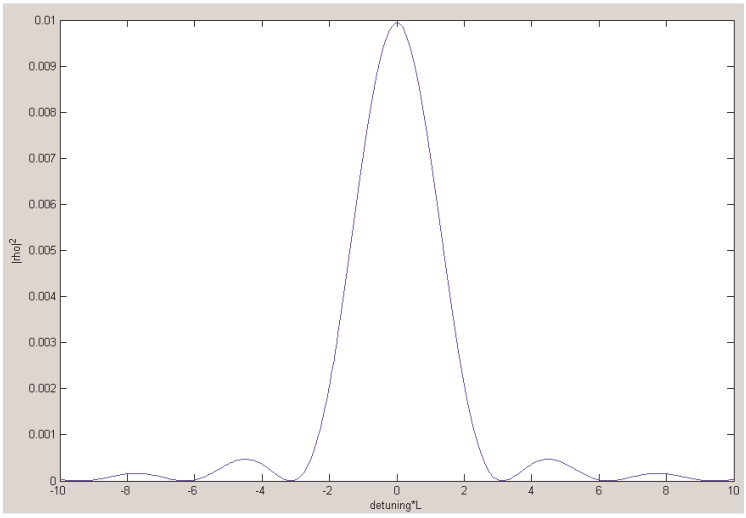

Figure 1 Reflection spectrum of a Bragg grating as function of detuning for ΩL=0.1

Using formula (A2.5) the intensity reflection of a Bragg grating is calculated. The detuning parameter δ is the difference of the wave vector of the mode at a particular wavelength with the one at Bragg resonance:

$$\delta = \beta - \beta_0 = \frac{2\pi n}{\lambda} - \frac{2\pi n}{\lambda_b} = \frac{2\pi n}{\lambda} - \frac{\pi}{\Lambda} \tag{2.2}$$

Figure 1 shows the result for the case of ΩL = 0.1. For this small mode coupling the spectrum is well described by the square of a sync function and the maximum equals $(\Omega L)^2$. For small reflec-

tion amplitudes the width of the resonance is independent of the coupling strength, but is only determined by the number N_g (= L/Λ) of periods present in the gating. The first zero points appear at $|\delta L| = \pi$. The relative wavelength difference of the zero points is therefore $\Delta\lambda/\lambda = 2/N_g$. For instance, for a grating length of 5 mm and a periodicity of 500 nm there are 10^4 periods, so that the full width at half maximum of the resonance is about 0.15 nm in wavelength.

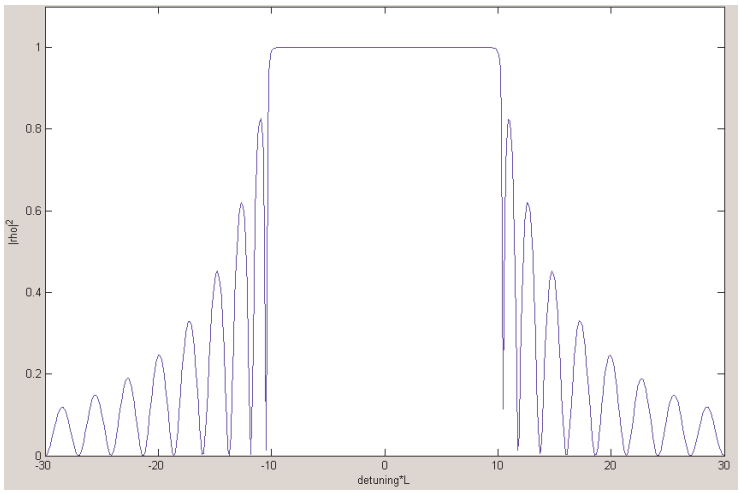

Figure 2 Reflection spectrum of a Bragg grating as a function of detuning for ΩL = 10.

Using equation (A2.5) the reflection of a homogenous Bragg grating with ΩL = 10 is calculated. In Figure 2 the reflection spectrum is plotted as a function of detuning for this high mode coupling coefficient. The maximum at zero detuning is very close to unity, and the width of the resonance is considerably broadened. For these two reasons (high maximum and broadened width) Bragg gratings with high mode coupling are used for fiber lasers. The sensitivity of the spectrum to external influences like temperature and strain is reduced for such broad spectra. Consequently, high mode coupling is not optimal for sensing, and in what follows below we will only consider the cases for small reflection coefficients.

For small signals the relation between the Fresnel reflection coefficient $\sigma(\delta)$ as function of detuning, i.e. wave vector, and the taper function of the grating as function of longitudinal position on the fiber is given by a Fourier transform. The derivation of this elegant relation is given in appendix (A3) and the result is repeated here:

$$\sigma(\delta) = -i\int_{-\infty}^{+\infty}\left(\Omega(z)e^{i\varphi(z)}\right)e^{-i2\delta z}dz \qquad (2.3)$$

The taper function is the product of the amplitude of the coupling coefficient $\Omega(z)$ and the phase factor containing $\varphi(z)$. Note the additional factor of 2 in the exponent. This factor of 2 stems from the fact that the reflected light has to travel back and forth along the fiber. In the example of Figure 1 the phase is zero everywhere and the coupling coefficient is constant and non zero over the range $-L/2 < z < L/2$. The Fourier transform of this block function gives the sync function, in agreement with our previous observation on the reflection spectrum of Figure 1. In general, however, the taper function is not constant. The first derivative of the phase is the chirp of the grating and signifies that the resonant condition is shifted to another wavelength. From Equation (2.3) it can be easily inferred that a constant chirp gives rise to the same Fourier transform as for zero chirp but shifted over a detuning of $\delta = 0.5 d\varphi(z)/dz$.

A constant strain gives rise to a constant chirp. From Equation (2.1) it is seen that a change in length of the fiber will induce a similar relative change in the period of the grating, and

consequently induce a shift in the resonant wavelength. The proportionality constant between strain ε and relative wavelength shift is smaller than unity due to the fact that the refractive index is also altered in a compensating way:

$$\frac{\Delta\lambda}{\lambda} = \zeta\varepsilon$$
$$\zeta = 1 - \frac{1}{2}n^2\left(p_{12} - \mu(p_{11} + p_{12})\right) \qquad (2.4)$$

The quantity μ is the Poisson ratio (about 0.16 for quartz) and p_{11} and p_{12} are strain optic coefficients (about 0.113 and 0.252 for quartz), so that the calibration constant ζ amounts to about 0.78. Knowing the relation between chirp and detuning, one can rewrite Equation (2.4) into a relation between chirp and strain:

$$\varepsilon(z) = -\frac{\Lambda}{2\pi\zeta}\frac{\partial\varphi(z)}{\partial z} \qquad (2.5)$$

We have now established a relation between strain and its influence on the reflection spectrum of a fiber Bragg grating via the relation between strain and chirp (Equation (2.5)) and a Fourier transform between taper function and Fresnel reflection coefficient (Equation (2.3)). In order to complete the mathematical framework for our forward calculations we only need to establish a relation between the strain and the shape of the fiber.

For a standard single mode fiber with its core in the central line of symmetry any change in shape will not induce strain in the core and consequently will not give rise to any spectral influences. Bending of the fiber induces compressive strain on the inside of the curvature and tensile on the outside. Because of the 3 dimensional nature of the shape we need to monitor the curvature in at least two orthogonal directions. We need to have two cores in the fiber both not centred in the middle at appreciable angles. Up till now, we have neglected any influence of temperature on the fiber Bragg gratings. In practice we should account for this effect, and hence we have to add a third core. For symmetry reasons and ease of fabrication we will put the three cores at nominally 120° with respect to each other.

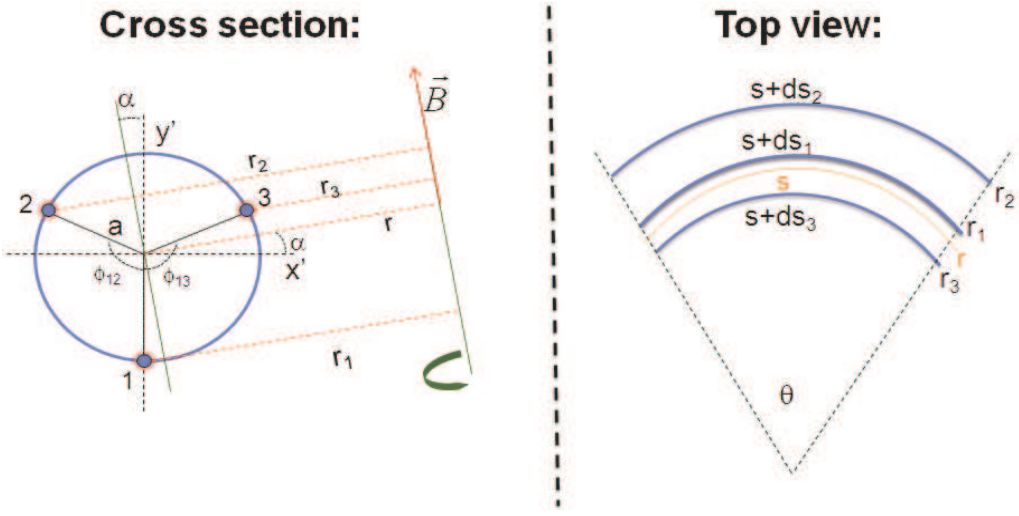

Figure 3 cross sectional and top view of a fiber with 3 cores

When a piece of fiber with nominal length *s* is bent over an angle θ, the three different cores will experience different elongations and strain owing to the differences in radii of curvature. From the top view of Figure 3 one can easily verify that there is a relation between the various strains and radii of curvature:

$$\theta = \frac{s + ds_j}{r_j} = s\frac{1 + \epsilon_j}{r_j} = \frac{s}{r} \quad j = 1,2,3 \tag{2.6}$$

From this and the geometry shown in cross sectional view of Figure 3 it is easily verified that the strain in a particular core and the nominal bend radius are related according to the following formulae:

$$\begin{aligned} \varepsilon_1 &= a\kappa sin(\alpha) \\ \varepsilon_2 &= a\kappa sin(\alpha + \Phi_{12}) \\ \varepsilon_3 &= a\kappa sin(\alpha - \Phi_{13}) \end{aligned} \tag{2.7}$$

Here, a is the distance of a core to the center, Φ_{ij} is the angle between the cores i and j, α is the angle between the radius of curvature and the internal coordinate system of the cross section, and $\kappa = 1/r$ is the curvature, i.e. the inverse of the radius of curvature. At any particular point along the fiber a bent can be described by a radius of curvature and an angle α. Those two parameters are equivalent to two independent strain values of two cores. By having three cores one introduces redundancy, necessary for the compensation of temperature effects. This common mode rejection is expressed by the following relationship between the three different strain quantities:

$$\varepsilon_1 \sin\Phi_{23} + \varepsilon_2 \sin\Phi_{13} + \varepsilon_3 \sin\Phi_{12} = 0 \tag{2.8}$$

Note, that the angles in Equation (2.8) are all taken positive, so that their sum equals 2π. For a regular spacing of the cores at 120° angles, the sum of the strain quantities is zero. At least one but at most two cores will be under tensile strain ($\varepsilon > 0$), and the other(s) under compressive strain ($\varepsilon < 0$). In the next chapter we will need the inverse relations of Equations (2.7) and calculate the radius of curvature and its direction from the strain values. For completeness we will state these relations here:

$$\tan\alpha = \frac{\varepsilon_{12}\sin\Phi_{13} + \varepsilon_{13}\sin\Phi_{12}}{\varepsilon_{12}(\cos\Phi_{13} - 1) - \varepsilon_{13}(\cos\Phi_{12} - 1)}$$
$$a\kappa = \frac{\varepsilon_{12}}{\sin(\alpha + \Phi_{12}) - \sin\alpha} = \frac{\varepsilon_{13}}{\sin(\alpha - \Phi_{13}) - \sin\alpha} = \frac{\varepsilon_{23}}{\sin(\alpha - \Phi_{13}) - \sin(\alpha + \Phi_{12})} \tag{2.9}$$

In Equations (2.9) the quantities ε_{ij} are defined as: $\varepsilon_{ij} = \varepsilon_j - \varepsilon_i$.

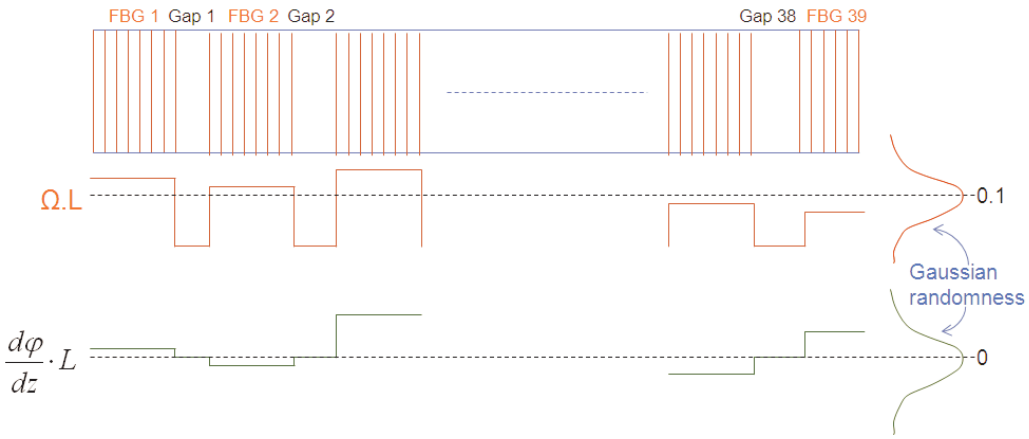

Figure 4 Distribution of Bragg gratings along the length of the fiber

For the forward calculation the shape of the fiber will give the radius of curvature and its direction at each point along the fiber. Using Equations (2.7) the strain in each of the cores can be calculated as a function of position along the fiber. Using these strain values and Equation (2.5) the induced chirp due to strain can be evaluated and substituted in the Fourier transform of

Equation (2.3) yielding the reflection spectra of the three different cores. Before doing so we have to set up the geometry of a fiber core. For practical applications the fiber will have a length of about one meter. It is impossible to create a Bragg grating over such a large length with reasonable amount of effort. Instead the fiber is subdivided in various parts each having a Bragg grating and separated by a small gap as depicted in Figure 4. Each of the Bragg gratings has a nominal length of 25 mm, a resonance at 1.55 micron and a coupling strength of 0.1 m^{-1}. The gaps in between the gratings are nominally 1 mm, so that 1 m of fiber contains 39 gratings. These quantities for the various gratings are allowed to have a Gaussian distribution around the nominal value, such that three times the standard deviation constitutes 10% of the nominal values for the length of gratings, the size of the gaps between the gratings and the amplitude of the coupling coefficient. Furthermore, the period of each of the gratings is allowed to vary. This is done by having a variation of the chirp (nominally zero for the unstrained fiber) with a value of three times the standard deviation equalling π m^{-1}. The resulting spectrum for the Fresnel reflection coefficient of the unstrained fiber is shown in Figure 5.

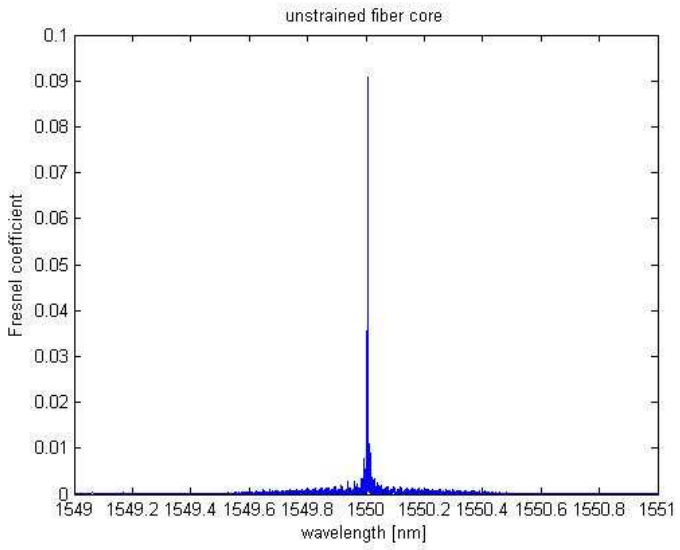

Figure 5 Absolute value of Fresnel reflection coefficient of the unstrained fiber with 39 Bragg gratings.

All the fine detail in the spectrum is not noise, but due to the small variations in the various parameters of the 39 gratings and clearly shows the deviation from the sync function for a single homogeneous Bragg grating. The maximum resonance has been reduced in amplitude somewhat and the width has increased more than an order of magnitude with respect to a single Bragg grating of 1 m length. Note that Figure 5 displays the Fresnel coefficient, meaning that the maximum reflectivity of the intensity is less than 1%. In the simulations we will assume that the three cores have identical spectra. There is no loss of generality, it makes it only easier to compare the spectra of the three different cores in the situation that strain is applied.

Below we will give the spectra of the three different cores of a 1 m long fiber when it is curved in a helical form. The radius of curvature is 10 cm and the pitch of 6.28 cm, so that the amount of turns is a little more than 1.5, the curvature κ is 10 m^{-1} and the torsion equals 1 m^{-1}. Although the radius of curvature is constant, its angle α with respect to the coordinate system of the cross section of the fiber is constantly increasing as given by Equation (A4.9). Substituting this result together with the value of the curvature in Equations (2.7) yields the strain as function of position. From Equation (2.5) the chirp can be inferred. This chirp due to shape is accounted for by an additional phase factor in the Fourier transform of Equation 2.3 on top of the existing phase factors due to the variation in the characteristics of the 39 gratings. The results for the three different cores are depicted in Figure 6.

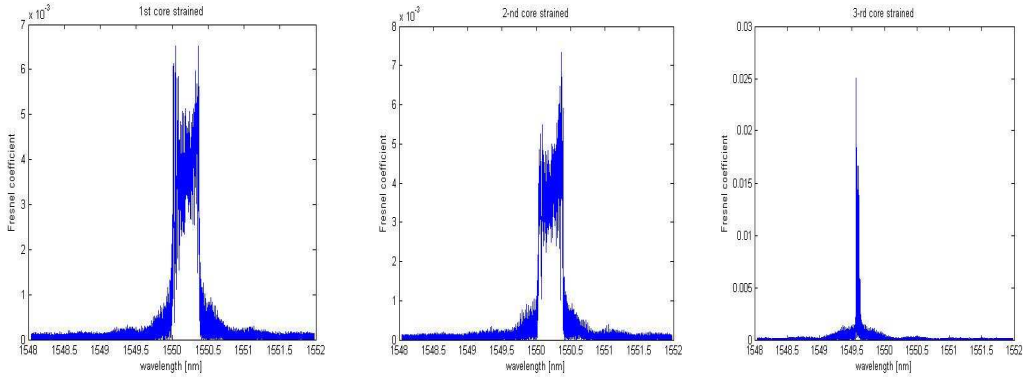

Figure 6 Spectra of Fresnel reflection coefficients for three cores of a fiber bent in a helix

The spectra of the three cores are vastly different from one another and from the spectrum of the unstrained case. The spectra of cores 1 and 2 are shifted to longer wavelengths meaning that these cores are tensile strained over a large portion of their length, while core 3 is shifted to smaller wavelength corresponding to compressive strain. The spectra for cores 2 and 3 are substantially broadened. The torsion of 1 m^{-1} caused the angle of the radius of curvature to change by 1 radian over the length of 1 m. The projection of the cores will alter in a sinusoidal way according to this angle. This gives a substantial variation in the magnitude of the effective strain in case this range lies close to the linear regime of the sinus. This is the case for cores 1 and 2. For core 3 the projection is at an extreme of the sinus function and within the range of 1 radian the variation in effective strain is not so large, yielding a much narrower spectrum. In the wings of the spectra a substantial amount of detail can be found. Although the amplitude is much smaller than the values at the (shifted) resonance, the information from the wings of the spectra is very important in the reconstruction of the shape of the fiber as will become apparent from the next chapter. Lastly, one should be aware of the fact that the Fresnel coefficients are complex quantities. We have only shown the amplitudes in Figure 5 and Figure 6, the values for the phase are equally important, but much more difficult to interpret. They should be taken into account in the reconstruction process to get a meaningful back Fourier transform.

3. Backward simulations: reconstruction of shape

We will now concentrate on the actual purpose of our endeavor. Let us assume that the spectra of a 3 core fiber have been measured with an interferometer both for the case of no strain (no bending) and for the case of a particular strain distribution, i.e. a particular shape. Assume that these spectra are given by Figure 5 and Figure 6, resp. By applying the inverse Fourier transform in accordance with Equation (2.3) one obtains the taper function. The amplitude of the taper function $\Omega(z)$ is not altered by the shape induced strain. All the shape information is contained in the phase of the taper function. By taking the difference of the phase in the strained and the unstrained case, and differentiating the result with respect to the coordinate along the fiber one obtains the chirp $d\varphi(z)/dz$ for each of the cores. Using Equation (2.5) one obtains the strain for each of the cores. Substituting the three strain distributions into Equation (2.9) yields the curvature κ and its angle α as function of position. This seems a straightforward process. There are, however, two difficulties in recovering the phase of the taper function. Firstly, the phase is only known on the interval $-\pi$ to π, and needs to be unwrapped in order to obtain a continuous, differentiable function. Secondly, the phase is not known in the gaps in between the Bragg gratings. These two effects are displayed in Figure 7.

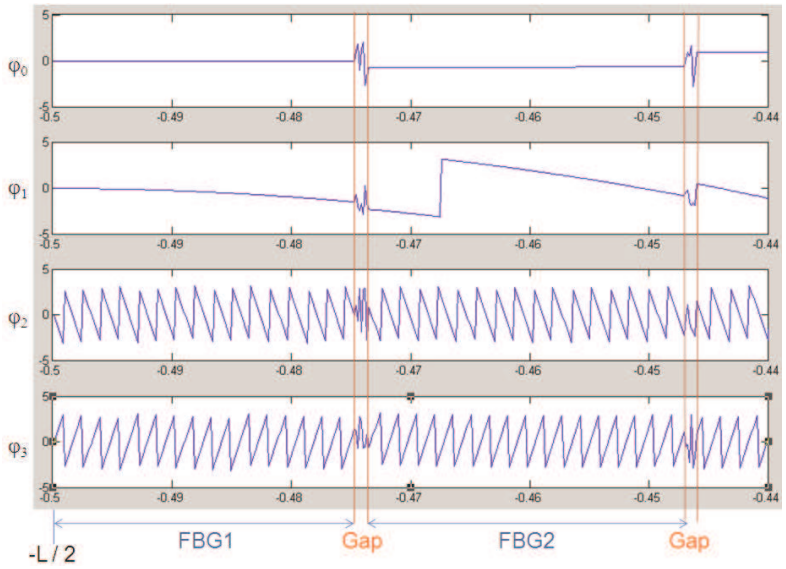

Figure 7 Zoomed in portion of the recovered phases of the taper function after inverse Fourier transforming

From the amplitude of the taper function it is known which points correspond to positions within the gap and the corresponding phase values are set to zero. Subsequently the difference with the unstrained reference is taken and the ensuing arrays are unwrapped and differentiated. The results are given in Figure 8. In the gap the chirp values are nonsensical and are removed from the arrays before prosecution of the next step. The next step is the calculation of the curvature and its angle as a function of position. The missing points in the gaps are interpolated with a quadratic spline function. For the curvature this is trivial since the helix has a constant curvature. For the helix the angle of the radius of curvature is a linear function and the interpolation is also straightforward. For more complicated shapes this interpolation may induce additional errors. This cannot be circumvented unless we allow for spatial overlap of the Bragg gratings.

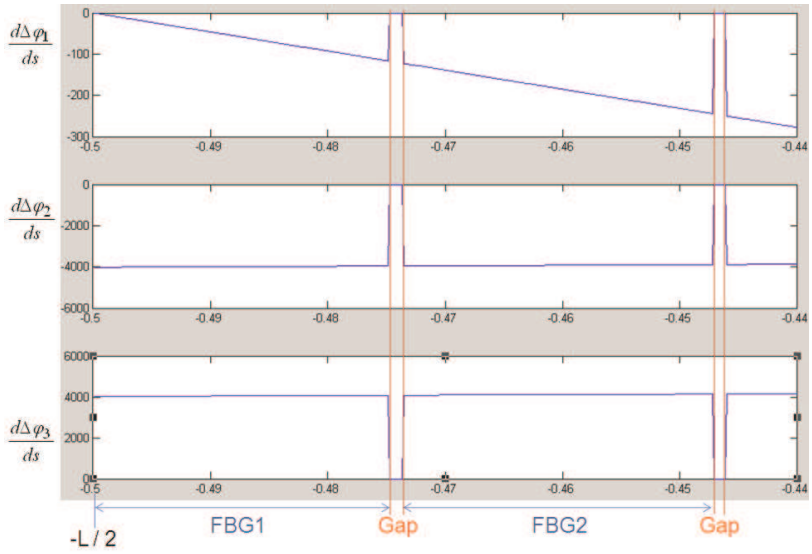

Figure 8 Zoomed in portion of the recovered chirp of the 3 cores in the fiber

Now that we have established the curvature and the torsion angle α as a function of position along the fiber, we 'only' have to reconstruct the shape. Consider the geometry of Figure 9 with a laboratory reference frame (X, Y, Z) and moving coordinate system (x'_i, y'_i, z'_i) along the fiber attached to the cross section of the fiber. At every point a new coordinate frame is established. Figure 9 depicts the situation of deriving point i+1 given input point i. The differential geometry frame (N, B, T) (see appendix A4 for the definitions) and the moving frame (x', y', z') are rotated over the torsion angle α in the (x', y') plane.

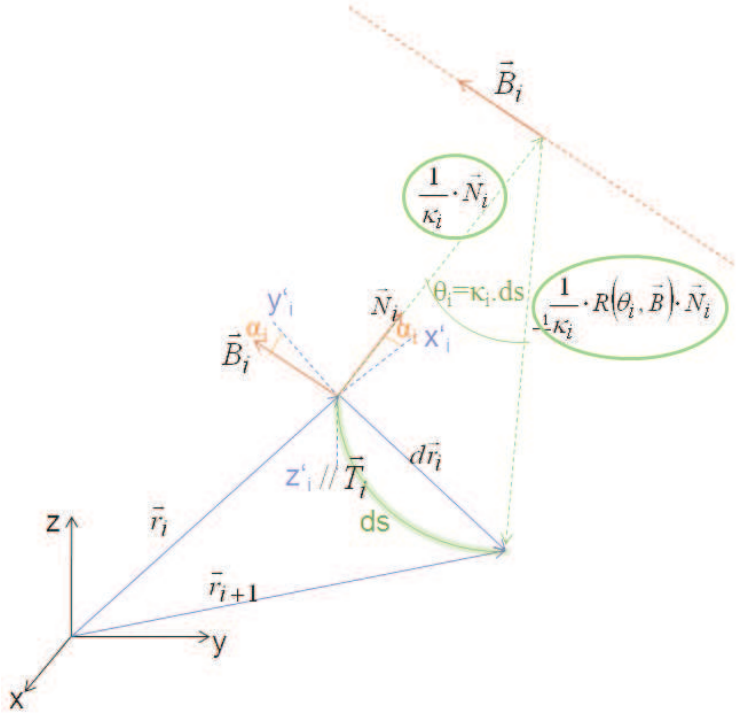

Figure 9 Lab coordinate system and fiber coordinate system showing a recursive reconstruction step.

At any point along the fiber the torsion angle α, the curvature κ and the step size ds are known from the inverse Fourier transform process described earlier. The transformation from point i to i+1 in the moving coordinate frame can be viewed as a rotation along the binormal axis ***B*** over an angle $\theta = \kappa ds$. Let us denote this rotation by $R(\theta,\boldsymbol{B})$. This means that the translation vector $\overrightarrow{dr'}$ in the moving frame is the difference between two radii of the same length but along two different directions subtending an angle θ.

$$d\vec{r}_i' = \frac{1}{\kappa_i}\vec{N}_i - \frac{1}{\kappa_i}\bar{\bar{R}}(\theta_i, \vec{B}_i)\cdot\vec{N}_i \qquad (3.1)$$

The relation between the fixed laboratory frame (X, Y, Z) and the moving frame (x', y', z') is given by the Jacobean A. This 3x3 matrix is an input of the first starting point and tells where the fiber begins in space and it's initially direction. The evolution of this Jacobean is governed by the same rotation operator $R(\theta,\boldsymbol{B})$:

$$\bar{\bar{A}}_{i+1} = \bar{\bar{A}}_i \cdot \bar{\bar{R}}(\theta_i, \vec{B}_i) \qquad (3.2)$$

Knowing the Jacobean one can easily calculate the position of the new point in the fixed laboratory frame given the previous point:

$$\vec{r}_{i+1} = \vec{r}_i + \frac{1}{\kappa_i}\bar{\bar{A}}_i \cdot \left(\bar{\bar{I}} - \bar{\bar{R}}(\theta_i, \vec{B}_i)\right)\cdot\vec{N}_i \qquad (3.3)$$

Note that although the Jacobean is a 3x3 matrix, it does not contain 9 independent variables, because it represents an orthonormal coordinate system. The Jacobean for the first point can be set by two orientation angles. The first point of the fiber has to be known also, constituting 3 additional boundary values at the start of the reconstruction.

Applying the recursive process of Equations (3.2) and (3.3) from the earlier obtained values for the curvature and the torsion angle, results in the reconstructed helix are depicted in Figure 10, and shown in red. The original helix is also drawn in Figure 10 in blue. The two curves are not distinguishable from one another, revealing the excellent shape recovery. Owing to the finite step size in the reconstruction and the missing phase values for the taper function in the gaps between the Bragg gratings, small deviations must exist between reconstructed and original shape.

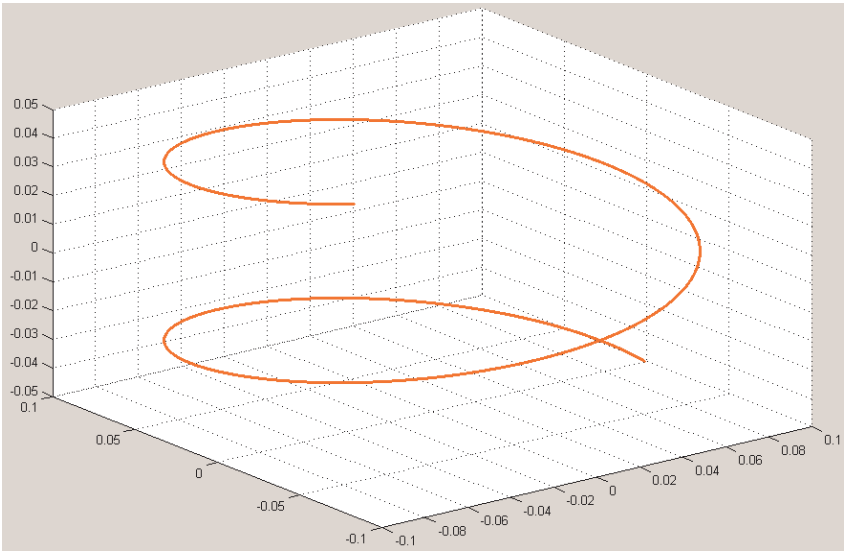

Figure 10 Reconstructed helical shape (red) and original (blue) of the fiber

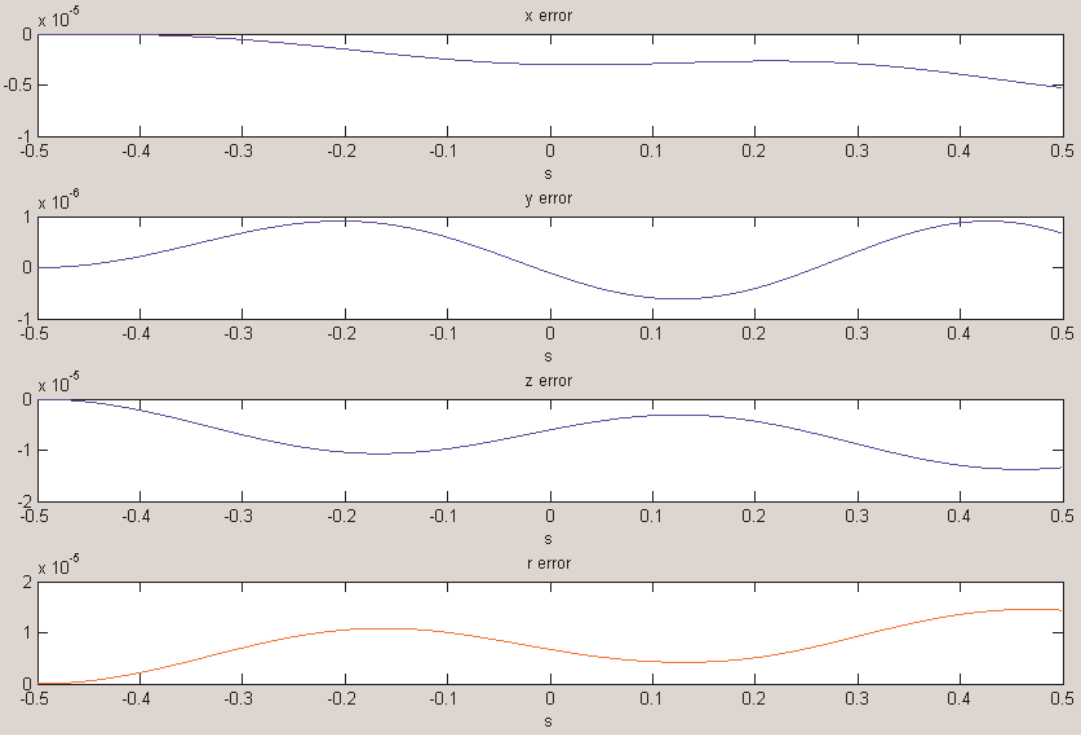

Figure 11 Errors in reconstruction of a standard helix

In Figure 11 the difference between reconstructed and original values for the three coordinates are plotted. The absolute value of the error is on the order of 10^{-5}m = 10μm. As the fiber is 1m long, the relative error is 10^{-5}. The error can be reduced by increasing the number of points, making the reconstruction more accurate. The accuracy scales quadratic with the number of points. The total amount of points in the Fourier transform calculations is quite substantial. However, the number of points within the 1 m fiber with Bragg gratings was on the order of 6000. From the above graph we see that the errors evolve in a periodic way in phase with the rotation of the helical form. In fact, the errors scale quadratically with the number of turns and also quadratically with the torsion.

In the last part of this chapter we will investigate a few variations on the same theme. What is the influence of noise on the data, what happens if we alter the shape in a more complicated form and what occurs when the three cores are not registered properly?

In this paragraph we would like to show what happens if noise is added to the reflection spectra before the inverse Fourier transformation. The additional noise has a Gaussian distribution and has a standard deviation in the order of 0.5% (compared to the maximum magnitude of the Fresnel reflection coefficient); the power of this noise is shared equally between the real and imaginary parts. The reconstruction algorithm remains in essence the same up till the gap points are removed from the strain distributions. As the strain curves are noisy an additional smoothing is performed. In the neighbourhood of a gap between two Bragg gratings a standard smoothing process is not adequate. Before and after each gap a few points are taken and fitted with two separate first order polynomial. Subsequently, the gap points are interpolated with a second order polynomial overlapping the two straight lines at each side of the gap. After this interpolation process smoothing is straightforward and the curvature and torsion angle are calculated in the usual way. Subsequently, the 3D shape is reconstructed and the result is given in Figure 12.

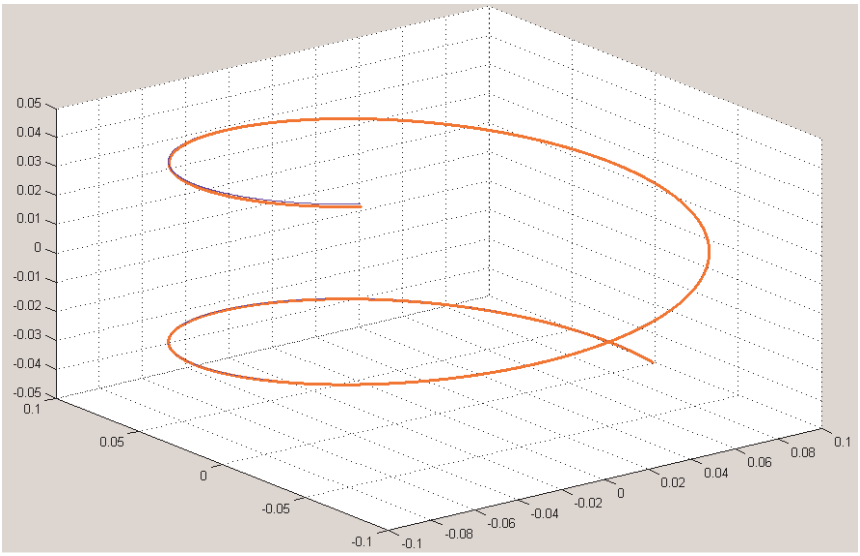

Figure 12 Reconstructed (red) and original (blue) helix form win the presence of 0.5% noise in the Fresnel reflection spectra.

The deviation between reconstruction and original data can already be seen in the 3D plot.

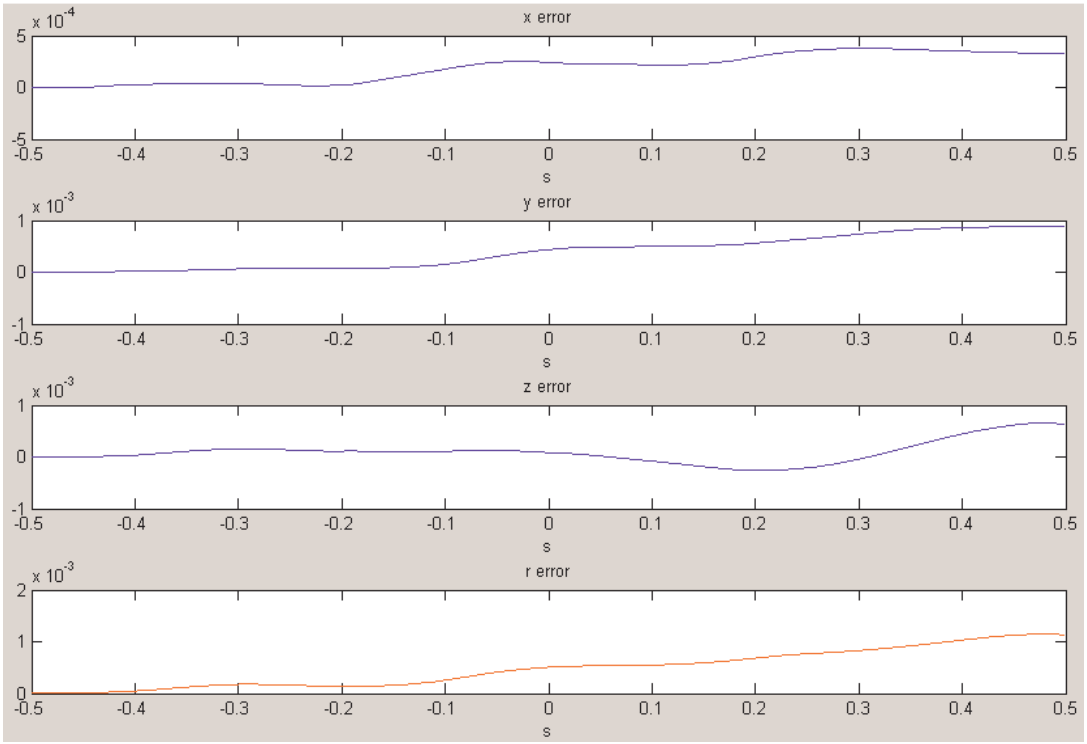

Figure 13 Error in the reconstruction of a standard helix when 0.5% noise is present on the Fresnel reflection spectra.

The noise of 0.5% causes the error to increase to 10^{-3}m = 1mm. The relative error amounts to 10^{-3}. For most medical applications the mm accuracy at the tip of the catheter would suffice. The above simulation thus shows that the measurement of the reflection spectra of fibers Bragg

gratings should have noise levels not exceeding 0.5%.

As a more complicated shape we have also reconstructed an expanded helix. For the formulae see appendix A6. The radius increases linearly with the length of the fiber. The form of the original and the reconstructed shape are shown in Figure 14.

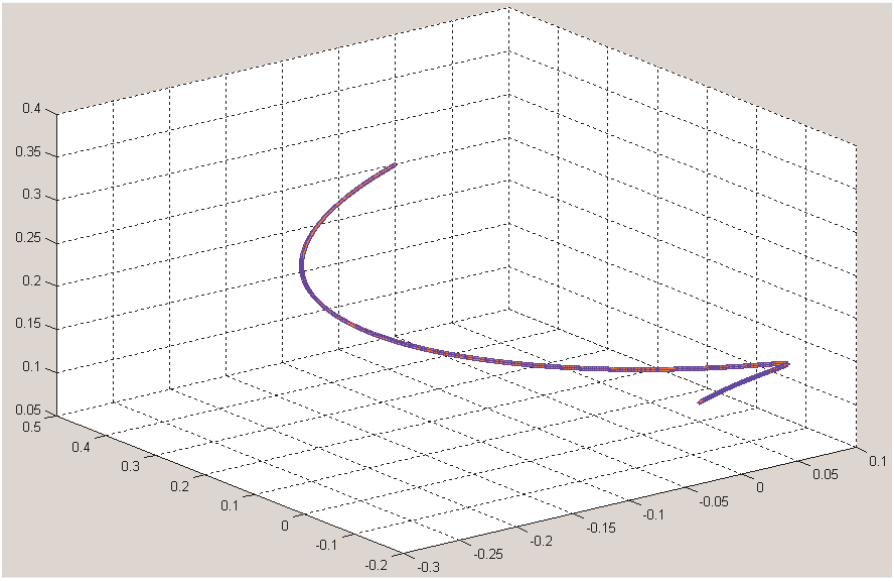

Figure 14 Original and reconstructed shapes of an expanding helix.

Again the original and the reconstructed shapes are indistinguishable from one another in Figure 14. The error, however, is substantially larger than in the case of the standard helix and amounts to 205 microns at most. At the tip of the fiber the error has reduced by almost a factor of 2 owing reduction in curvature. Due to this more involved shape the error at the tip is an order of magnitude larger than for the standard helix.

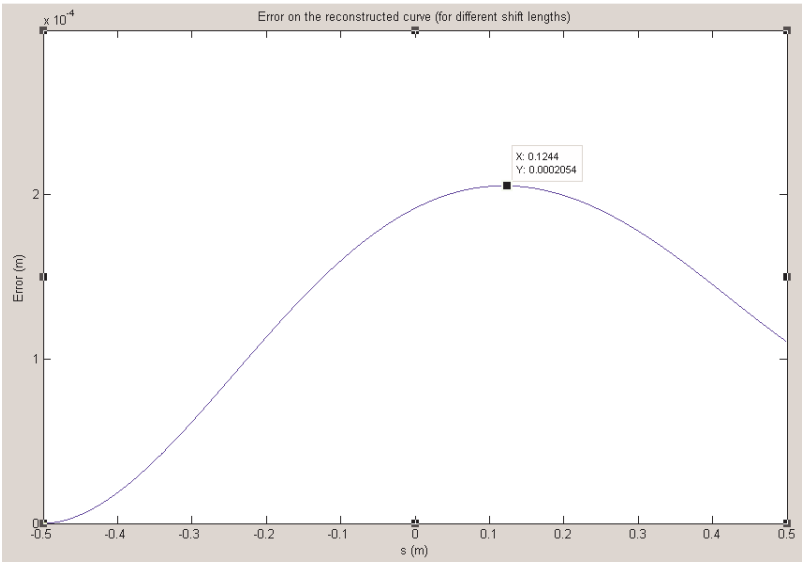

Figure 15 Error in the reconstruction of a 1m long expanding helix

Similarly as for the standard helix, we can decrease the error further by increasing the number of points thus decreasing the step size. However, when there is noise on the reflection spectra,

smaller steps give rise to larger errors in the derivative of the phases and consequently strain value. This can be repaired by more severe smoothing algorithms. The latter will have the effect that variations in curvature and/or torsion on a small length scale will get lost. There's one particular point about the expanding helix: at the beginning of the fiber the curvature and the torsion are very large and their derivatives are also sizeable. Consequently, an error in the orientation of the first few steps has a huge impact on the error on the distal points.

In practice, a fiber with multiple cores needs a fan out system. Such a fan out is fusion spliced to the multicore fiber and on the other side has multiple single core fibers with connectors. Those single core fibers can have different lengths. This can give rise to registration errors. In order to simulate this, we shifted the 3 cores with respect to one to another over a few mm (that is to say several points) and we evaluated the impact on the reconstruction.

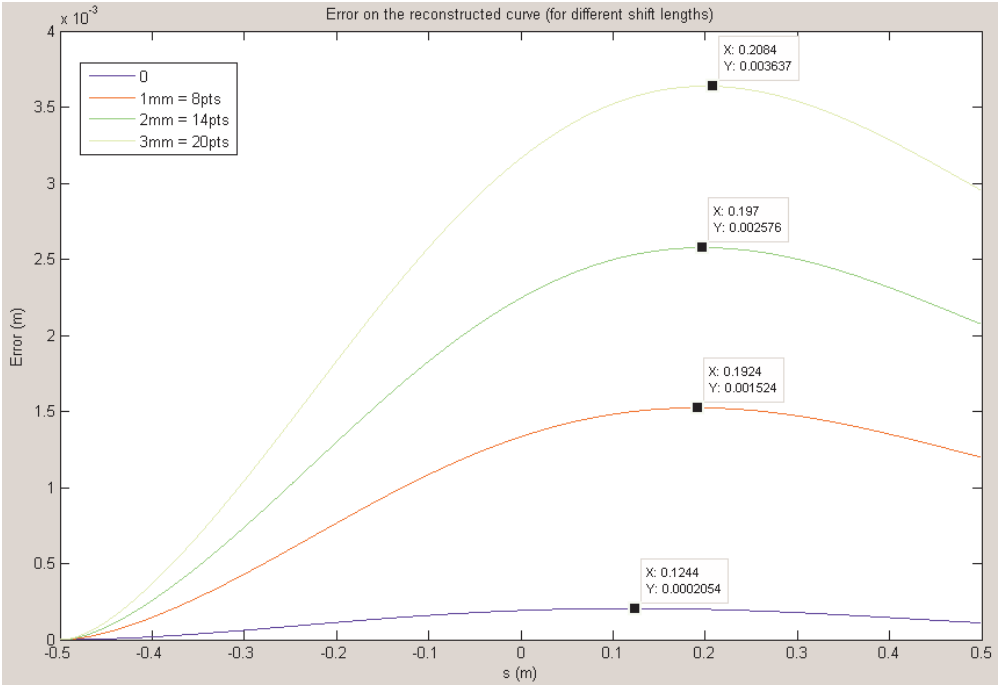

Figure 16 Reconstruction errors for an expanding helix when the different cores are having different lead lengths and are misaligned with respect to each other.

The form of the error in the reconstruction stays the same. The maximum error increases linearly with the amount of shift between the cores with a slope close to unity. Consequently, in order to keep the accuracy of the reconstruction around 1 mm one should measure and calibrate the fan out system to a precision better than 1 mm.

4. Conclusions

The modelling of the Bragg sensors to reconstruct the geometry of a fiber has been accomplished with good results. The relative errors are in the order of 0.001% for a fiber bended as a standard helix and 0.02% for the expanding helix.
The influence of noise in the reflection spectra is simulated for the case of a fiber bended as a standard helix. The error in the reconstruction increases to 0.1% (factor of 100 compared to the case without noise) with a noise level of only 0.5% in magnitude. This sets a standard for the accuracy of experimental data.

In the example of the expanding helix, we simulated the problem of registration of multiple cores by shifting them with respect to one another The error increases linearly with the length of the shift, for a shift in the order of 1 mm the error amounts to 0.15% (factor of 7.5 compared to the expanding helix without registration problem).

There remains a substantial amount of future work. A list of items that needs to be addressed comprises the following:

- Bending of the fiber causes birefringence. This birefringence will change the optical path length causing a shift between measured taper functions and those obtained from the reference measurement without strain. Furthermore, it will give rise to polarization fading of the signals.
- In the reconstruction algorithm given in this report torque has not been taken into account. In practice, torque can probably not be avoided.
- Phase noise of the optical source and non-linearity in the frequency scan will give rise to errors. The influence of this non ideal behavior needs to be evaluated.
- Would the reconstruction algorithm be the same in the case of Rayleigh scattering? The advantage of Bragg gratings is that the signals are much larger and that additional patch cord length between interrogation console and tether can be accounted for. This last point stems from the fact that that there is no negative space degeneracy, since the patch cords do not contain Bragg gratings. The disadvantage of Bragg gratings is the presence of gaps. This generates uncertainties is the comparison of reference data and strained data which is augmented by the presence of birefringence.

5. Acknowledgements

We would like to acknowledge the fruitful and inspirational discussions with the other members of the smart delivery project *in casu* Heinrich von Busch, Ray Chan, Martin van der Mark and Robert Manzke.

References

[1] H. Kogelnik, FILTER RESPONSE OF NONUNIFORM ALMOST-PERIODIC STRUCTURES, *Bell System Technical Journal*, vol. 55, pp. 109-126, 1976

A Appendices

A.1 Coupled wave equations

In this appendix we will derive a set of coupled wave equations describing the forward and backward travelling waves in a fiber with non-uniform, almost periodic structures. The approach that we take is based on the work of Kogelnik [1]. Consider a single mode fiber with a refractive index in the core, n_{co}, and a refractive index in the cladding, n_{cl}, and a core radius, r_c. The normalized frequency, V, describes the single or multimode behaviour of the fiber. The normalized frequency can be calculated with:

$$V = \frac{2\pi r_c}{\lambda}\sqrt{{n_{co}}^2 - {n_{cl}}^2} \tag{A1.1}$$

For values smaller than 2.405 (the first zero point of the Bessel function J_0) the fiber is single mode. For a step index fiber the mode volume is given by $4V^2/\pi^2$. For values of the normalized frequency larger than 5, half of its square is a good measure for the amount of modes available. Here we will adhere to single mode behaviour. The normalized frequency for the fundamental mode of a single mode fiber is also a good measure for the relative power in the core:

$$M^2 = 1 - \frac{1}{V^2} \tag{A1.2}$$

The effective refractive index of the fundamental mode is a weighted average of the refractive index of core and cladding. The weight coefficient is off course the relative power in the core.

$$n_{eff} = M^2 n_{co} + (1 - M^2) \cdot n_{cl} \tag{A1.3}$$

Assume that the characteristics of the fundamental mode of a single mode fiber are known, and that a non-uniform, almost periodic structure is added to the core as a perturbation. The wave equation is as usual:

$$\nabla^2\vec{\mathrm{E}} - \mu_0\varepsilon_0\frac{\partial^2\vec{\mathrm{E}}}{\partial \mathrm{t}^2} = \mu\frac{\partial^2\vec{\mathrm{P}}(\vec{\mathrm{r}},\mathrm{t})}{\partial \mathrm{t}^2} \tag{A1.4}$$

The polarization P has two contributions, Firstly, the unperturbed guided fiber mode and a second small contribution from the periodic perturbation:

$$\vec{\mathrm{P}}(\vec{\mathrm{r}},\mathrm{t}) = \vec{\mathrm{P}}_0(\vec{\mathrm{r}},\mathrm{t}) + \vec{\mathrm{P}}_{\mathrm{pert}}(\vec{\mathrm{r}},\mathrm{t}) \tag{A1.5}$$

The phenomenological equation describing the relation between the electric field and the unperturbed polarization is given by:

$$\vec{\mathrm{P}_0}(\vec{\mathrm{r}},\mathrm{t}) = (\varepsilon(\vec{\mathrm{r}}) - \varepsilon_0)\vec{\mathrm{E}}(\vec{\mathrm{r}},\mathrm{t}) \tag{A1.6}$$

The solution to the wave equation (A1.4) for the unperturbed case of equation (A1.6) constitutes of forward and backward travelling waves, and can in general be written as.

$$\vec{E_0}(\vec{r},t) = \vec{A}(x,y)\left[R(z)\mathrm{e}^{\mathrm{i}(\omega \mathrm{t}-\beta \mathrm{z})} + \mathrm{S}(\mathrm{z})\mathrm{e}^{\mathrm{i}(\omega \mathrm{t}+\beta \mathrm{z})}\right] \tag{A1.7}$$

The quantity *A(x,y)* describes the field distribution over the cross section of the fiber and β is the propagation constant along the length of the fiber, i.e. the wave vector with effective refractive index as given by equation (A1.3).Substituting the general solution for the forward and backward travelling wave each separately in the unperturbed wave equation, and applying the slowly varying amplitude approximation, i.e. $|\beta R(z)| \gg |\partial R(z)/\partial z|$ and $|\beta S(z)| \gg |\partial S(z)/\partial z|$, one obtains:

$$\left(\frac{\partial^2}{\partial x^2}+\frac{\partial^2}{\partial y^2}-\beta^2\right)A(x,y)R(z)+\mu\varepsilon(\vec{r})\omega^2A(x,y)R(z)=0$$
$$\left(\frac{\partial^2}{\partial x^2}+\frac{\partial^2}{\partial y^2}-\beta^2\right)A(x,y)S(z)+\mu\varepsilon(\vec{r})\omega^2A(x,y)S(z)=0 \qquad \text{(A1.8)}$$

Owing to the slowly varying amplitude approximation and the homogeneity of the dielectric constants of the fiber in the longitudinal direction, the above equations (A1.8) do not contain any z-dependence (those will come from adding perturbations). The quantities *R(z)* and *S(z)* can be divided out of equations (A1.8). This procedure results in a differential equation for the mode profile *A(x,y)*.

$$\left(\frac{\partial^2}{\partial x^2}+\frac{\partial^2}{\partial y^2}-\beta^2\right)A(x,y)+\mu\varepsilon(x,y)\omega^2A(x,y)=0 \qquad \text{(A1.9)}$$

We will assume that the solution to equation (A1.9) is known. From this known solution, the influence of an additional variation of the dielectric constant in the longitudinal direction is calculated using first order perturbation theory. To this end, the homogeneous solution (A1.7) is substituted on the left hand side of equation (A1.4) and on the right hand side the perturbed polarization is substituted. In formula form this means:

$$\nabla^2\overrightarrow{\mathrm{E}_0}-\mu_0\varepsilon(\vec{\mathrm{r}})\frac{\partial^2\overrightarrow{\mathrm{E}_0}}{\partial \mathrm{t}^2}=\mu\frac{\partial^2\overrightarrow{\mathrm{P}_{\mathrm{pert}}}(\vec{\mathrm{r}},\mathrm{t})}{\partial \mathrm{t}^2}$$

with

$$\overrightarrow{\mathrm{P}_{\mathrm{pert}}}(\vec{\mathrm{r}},\mathrm{t})=\Delta\varepsilon(\vec{\mathrm{r}})\cdot\vec{E}(\vec{r},t) \qquad \text{(A1.10)}$$

and

$$\Delta\varepsilon(\vec{\mathrm{r}})=\Delta\varepsilon(\mathrm{x},\mathrm{y})\left(e^{i(Kz+\varphi)}+e^{-i(Kz+\varphi)}\right)$$

The periodicity of the variation of the dielectric constant is given by the wave vector *K* and the phase φ. The variation is purely in the z-direction and will give rise to a functional dependence of *R(z)* and *S(z)* on this longitudinal direction. Retaining only first order derivatives of *R(z)* and *S(z)* one obtains from (A1.10):

$$-2i\beta A(x,y)\left[\frac{\partial R}{\partial z}e^{-i\beta z}-\frac{\partial S}{\partial z}e^{i\beta z}\right]$$
$$=-\omega^2\mu\Delta\varepsilon(\mathrm{x},\mathrm{y})\left(e^{i(Kz+\varphi)}+e^{-i(Kz+\varphi)}\right)A(x,y)\left(R(z)\mathrm{e}^{-\mathrm{i}\beta\mathrm{z}}+\mathrm{S}(\mathrm{z})\mathrm{e}^{\mathrm{i}\beta\mathrm{z}}\right) \qquad \text{(A1.11)}$$

Multiplying equation (A1.11) with the complex conjugate of the mode profile, A*(x,y) and integrating over the cross section of the mode leaves only functions that exhibit z-dependence:

$$-2i\beta\left[\frac{\partial R}{\partial z}e^{-i\beta z}-\frac{\partial S}{\partial z}e^{i\beta z}\right]=-K\left(e^{i(Kz+\varphi)}+e^{-i(Kz+\varphi)}\right)\left(R(z)\mathrm{e}^{-\mathrm{i}\beta\mathrm{z}}+\mathrm{S}(\mathrm{z})\mathrm{e}^{\mathrm{i}\beta\mathrm{z}}\right)\Omega \qquad \text{(A1.12)}$$

In equation (A1.12) use is made of the fact that the mode profile is a normalized function, meaning:

$$\iint_{-\infty}^{+\infty}|A(x,y)|^2\,dxdy=1 \qquad \text{(A1.13)}$$

Furthermore, the following quantities have been defined:

$$\Omega\equiv\frac{\omega^2\mu}{K}\iint_{-\infty}^{+\infty}\Delta\varepsilon(\mathrm{x},\mathrm{y})|A(x,y)|^2\,dxdy$$
$$2\beta_0\equiv K=\frac{2\pi}{\Lambda} \qquad \text{(A1.14)}$$
$$\delta\equiv\beta-\beta_0$$

The physical meaning of these quantities is: Ω is the coupling coefficient between the forward and backward travelling wave, β_0 is the wave vector at resonance ($2\pi/\lambda_{Bragg}$) and δ is the detuning. In equation (A1.12) both the resonance wave vector and the actual wave vector are present. It is more convenient to solve the coupling of the forward and backward travelling waves as a function of the detuning parameter. In order to do so, we define new, reduced quantities for the amplitudes of the forward and backward travelling waves. They differ from the original ones by only a phase factor:

$$\begin{aligned} R(z)e^{-i\beta z} &\equiv \hat{R}(z)e^{-i\beta_0 z} \\ S(z)e^{i\beta z} &\equiv \hat{S}(z)e^{i\beta_0 z} \end{aligned} \qquad \text{(A1.15)}$$

Substituting equations (A1.15) into equation (A1.12) and collecting terms with the same periodicity yields two coupled equations for the amplitudes of the forward and backward travelling waves:

$$\begin{aligned} \frac{\partial \hat{R}}{\partial z} + i\delta\hat{R}(z) &= -i\Omega\hat{S}(z)e^{-i\varphi(z)} \\ \frac{\partial \hat{S}}{\partial z} - i\delta\hat{S}(z) &= i\Omega\,\hat{R}(z)e^{i\varphi(z)} \end{aligned} \qquad \text{(A1.16)}$$

From the differential equations (A1.16) it is clear why Ω is called the coupling coefficient. At zero detuning and zero phase, the coupling is maximal and the one wave will grow exponentially at the expense of the other with a gain/decay length equalling the inverse of the coupling coefficient. Note, that the phase factor φ is not the phase of one of the light waves but the phase of the periodicity of the perturbation in the dielectric constant, e.g. the phase of the Bragg periodicity. This phase factor does not need to be constant and can be chirped with the effect that the resonance condition can be shifted away from β_0. For most applications it is more convenient to solve the set of coupled equations as a single differential equation for the reflection coefficient. An effective, reduced reflection coefficient $\rho(z)$ is defined as:

$$\begin{aligned} \rho(z) &\equiv \frac{\hat{S}(z)}{\hat{R}(z)}e^{-i\varphi(z)} = \sigma(z)e^{i\left(2\delta z-\varphi(z)\right)} \\ \sigma(z) &\equiv \frac{S(z)}{R(z)} = \frac{\hat{S}(z)}{\hat{R}(z)}e^{-i2\delta z} \end{aligned} \qquad \text{(A1.17)}$$

The true Fresnel reflection coefficient $\sigma(z)$ is related to the reduced reflection coefficient by a phase factor, which vanishes for zero detuning and at the beginning of the structure. Combining equations (A1.16) and using the equation (A1.17) for the reduced reflection coefficient we arrive at our final result:

$$\frac{\partial\rho}{\partial z} = i\left(2\delta - \frac{\partial\varphi}{\partial z}\right)\rho(z) + i\Omega(z)(\rho^2(z)+1) \qquad \text{(A1.18)}$$

Equation (A1.18) is a differential equation of the Riccati type. As input the phase $\varphi(z)$ and coupling coefficient $\Omega(z)$ have to be known. Their functional behaviour reflects e.g. the presence of multiple Bragg reflectors, i.e. different strength of the coupling on various positions and gaps with no coupling in between. Furthermore, with the phase the interference of the reflected wave can be adjusted and with the chirp (derivative of the phase) the resonance wavelength can be tuned. Given a fiber length L, usually the coordinate along the fiber runs from $-L/2$ to $L/2$, and the boundary conditions are taken such that $R(z=-L/2)=1$ and $S(z=L/2)=0$ meaning that light is only entering from one end and not from the other. Consequently, $\sigma(L/2)=\rho(L/2)=0$, and one is interested what the value of the (Fresnel) reflection coefficient is at the beginning of the fiber, i.e. $\sigma(-L/2)$ and/or $\rho(-L/2)$.

A.2 Exact solution of the Riccati equation

The Riccati equation (A1.18) describing the reflection from a nearly periodic structure in a single mode fiber is non-linear. Only in a few cases it can be solved analytically. One example is the case of a homogeneous Bragg reflector with coupling coefficient which is constant throughout the full length of the fiber, but arbitrary magnitude and no position dependence of the phase of the modulation. Instead of solving (A1.18) we will try to find solutions for the set of coupled equations (A1.16) in which we take $\varphi(z)=0$. The trial solution is a set of *sinh* and *cosh* functions:

$$\begin{aligned} \hat{R}(z) &= a\cosh\left(\gamma\left(z-\frac{L}{2}\right)\right)+b\sinh\left(\gamma\left(z-\frac{L}{2}\right)\right) \\ \hat{S}(z) &= c\cosh\left(\gamma\left(z-\frac{L}{2}\right)\right)+d\sinh\left(\gamma\left(z-\frac{L}{2}\right)\right) \\ \gamma &= \sqrt{{\Omega_0}^2-\delta^2} \end{aligned} \tag{A2.1}$$

From the boundary conditions we have to find the constants *a, b, c* and *d*. Subsequently, the reflection coefficient has to be calculated from the ratio of *R(z)* and *S(z).* The boundary condition is $S(L/2)=0$, i.e. only input from the beginning of the fiber with normalized amplitude. This boundary condition immediately implies $c=0$. Substitution of the trial functions (A2.1) with $c = 0$ into the set of coupled equations (A1.16) gives:

$$\begin{aligned} (b\gamma+i\delta a)\cosh\left(\gamma\left(z-\frac{L}{2}\right)\right) &= -(a\gamma+i\delta b+i\Omega_0 \mathrm{d})\sinh\left(\gamma\left(z-\frac{L}{2}\right)\right) \\ (d\gamma-i\Omega_0 \mathrm{a})\cosh\left(\gamma\left(z-\frac{L}{2}\right)\right) &= i(\delta d+\Omega_0 \mathrm{b})\sinh\left(\gamma\left(z-\frac{L}{2}\right)\right) \end{aligned} \tag{A2.2}$$

The equations (A2.2) have to be valid for any value of the space coordinate *z*. Let us choose conveniently $z = L/2$, where the *sinh* function vanishes. Consequently, the multiplying factors of the cosh functions have to be zero.

$$\begin{aligned} b\gamma+i\delta a &= 0 \\ d\gamma-i\Omega_0 \mathrm{a} &= 0 \end{aligned} \tag{A2.3}$$

It can easily be verified that with the relations (A2.3) between *a*, *b* and *d* it also holds that the multiplying factors of the *sinh* functions vanish. When all the four multiplying factors are zero, the equations (A2.2) hold for any value of *z*. After substitution of the relations (A2.3) into the trial functions (A2.1) and taking the ratio of S and R one obtains the expression for the reflection coefficient. At the beginning of the fiber it equals:

$$\begin{aligned} \rho\left(\delta, z=-\frac{L}{2}\right) &= \frac{\hat{S}(-L/2)}{\hat{R}(-L/2)} = -i\frac{\Omega_0\sinh(\gamma L)}{\gamma\cosh(\gamma L)+i\delta\sinh(\gamma L)} \\ \sigma\left(\delta, z=-\frac{L}{2}\right) &= -i\frac{\Omega_0\sinh(\gamma L)}{\gamma\cosh(\gamma L)+i\delta\sinh(\gamma L)}e^{i\delta L} \end{aligned} \tag{A2.4}$$

Usually, one is not interested in the reflection coefficient for the amplitudes but only in the reflection coefficient for the intensity:

$$\mathcal{R} = \rho\rho^* = \sigma\sigma^* = \frac{{\Omega_0}^2\sinh^2(\gamma L)}{\gamma^2\cosh^2(\gamma L)+\delta^2\sinh^2(\gamma L)} \tag{A2.5}$$

Two interesting limited cases: Firstly, for zero detuning, $\delta = 0$ and $\gamma = \Omega$, equation (A2.5) gives a $\tanh^2(\Omega L)$. Secondly, for small values of ΩL the reflection coefficient equals $\Omega^2 L^2\,\mathrm{sinc}^2(\delta L)$.

A.3 Small signal approximation

The Riccati equation (A1.18) does not contain a phase factor owing to the fact that we have used a reduced reflection coefficient ρ instead of the Fresnel reflection coefficient σ. From (A1.17) it is clear that the ratio between these two coefficients is only a phase factor $exp[i(2\delta z-\varphi)]$. The Riccati equation in terms of the Fresnel reflection coefficient reads:

$$\frac{\partial \sigma}{\partial z} = i\Omega(z)\left(\sigma(z)^2 e^{i(2\delta z-\varphi(z))} + e^{-i(2\delta z-\varphi(z))}\right) \qquad \text{(A3.1)}$$

When the reflectivity is very small $\sigma(z)<<1$ the first term on the right hand side of equation (A3.1) is negligible small with respect to the second term. In that case the solution for the Fresnel reflection coefficient at the beginning of the fiber can formally be solved and is given by:

$$\sigma(\delta) = -i\int_{-L/2}^{+L/2}\left(\Omega(z)e^{i\varphi(z)}\right)e^{-i2\delta z}dz \qquad \text{(A3.2)}$$

The integration boundaries can be replaced by -∞ and +∞, since Ω is zero outside the fiber, i.e. for $|z| > L/2$. Consequently, the reflection coefficient of a fiber containing almost periodic structures is given by a Fourier transform of the taper function of these structures. The taper function contains an amplitude describing the coupling between forward and backward travelling wave and a phase factor. The first derivative of the phase factor is the chirp and has the physical meaning that the resonance condition at that part of the structure has shifted to another wavelength. When the taper function is real, i.e. when the phase is small ($\varphi(z)=0$), the Fourier transform will result in an even function. In that case the reflection coefficient is the same for positive and negative detuning values. Note the factor of 2 in the exponent of the Fourier transform. This factor of 2 is a consequence of the fact that the light has to travel back and forth over the fiber length.

A.4 Differential geometry

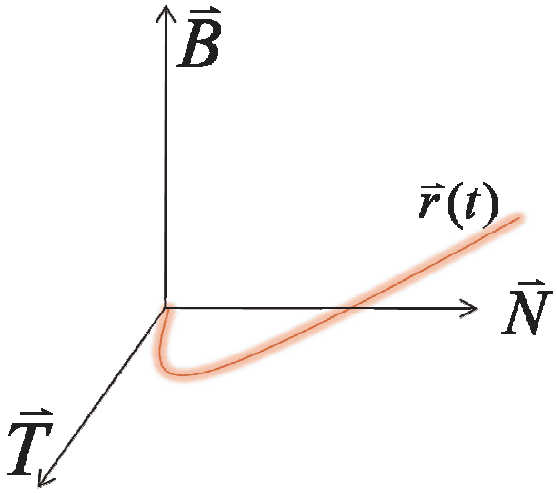

Figure 17 Frenet frame

In this section we will recall the basics of differential geometry concerning 3 dimensional curves. Consider such a curve for which the coordinates *x*, *y* and *z* are a function of a parameter *t*:

$$\vec{r}(t) = \begin{pmatrix} x(t) \\ y(t) \\ z(t) \end{pmatrix} \tag{A4.1}$$

The parameter *t* could be the distance travelled over the curve, but in general this is not the case. This means that we have to normalize the upcoming parameters with the length of the curve. The distance travelled along the curve is:

$$s(t) = \int_0^t \|\vec{r}'(\tilde{t})\| \, d\tilde{t} = \int_0^t \sqrt{\vec{r}'(\tilde{t}) \cdot \vec{r}'(\tilde{t})} \, d\tilde{t} \tag{A4.2}$$

Here the prime denotes that one has to take the derivative. The direction of the slope of the curve at any point in space is given by its tangent. The tangent is a normalized vector:

$$\vec{T}(t) = \frac{\vec{r}'(t)}{\|\vec{r}'(t)\|} \tag{A4.3}$$

The radius of curvature of the curve lies in the direction of the normal vector $\vec{N}(t)$, which can be calculated with:

$$\kappa(t)\vec{N}(t) = \frac{\vec{T}'(t)}{\|\vec{r}'(t)\|} = \frac{\vec{T}'(t)}{s'(t)} \tag{A4.4}$$

The normal vector describes the change of the tangent vector, and is also a unit vector. Hence, the normal vector $\vec{N}(t)$ is orthogonal to the tangent vector $\vec{T}(t)$ as its name already suggests. The plane subtended by the two vectors is called the oscillating plane. The scalar quantity $\kappa(t)$ is called the curvature i.e. the inverse of the radius of curvature. An orthonormal coordinate system is obtained by defining a binormal vector which is the vector product of the tangent and the normal vector:

$$\vec{B}(t) = \vec{T}(t) \times \vec{N}(t) \tag{A4.5}$$

The coordinate system $\vec{T}(t), \vec{N}(t), \vec{B}(t)$ is called the Frenet coordinate system and is a moving frame of reference of the 3 dimensional curve. In case the curve is only 2 dimensional the oscillating plane will have a constant orientation with respect to an external laboratorium frame. The binormal vector orthogonal to that plane will not change. For a 3 dimensional curve, however, the binormal vector will alter its direction; the magnitude of this change is called the torsion τ. Since the binormal vector is a unit vector, its derivative must lie in the oscillating plane. The normal vector is the derivative of the tangent. Consequently, it is easily verified using equation (A4.5) that the derivative of the binormal is orthogonal to the tangent. As a result the change of the binormal vector is in the direction of the normal vector:

$$\frac{\vec{B}'(t)}{\|\vec{r}'(t)\|} = -\tau(t)\vec{N}(t) \tag{A4.6}$$

In equation (A4.3), (A4.4) and (A4.6) an additional normalization factor appears: $\|\vec{r}'(t)\| = s'(t)$. This is caused by the fact that we take the derivatives with respect to the parameter *t*, and not the curve length *s*. For those cases where the curve can be parameterized in units of its distance travelled along the curve, this normalization factor is unity.

The evolution of all vectors in the Frenet frame can be described by the same differential equation, the so-called Darboux equation:

$$\vec{v}' = \vec{\omega} \times \vec{v}$$
$$\omega = \tau\vec{T} + \kappa\vec{B} \qquad \text{(A4.7)}$$

Torsion is a rotation around the tangent and curvature a rotation around the binormal. Applying the Darboux equation to the three basic vectors tangent, normal and binormal, one obtains the well-known Frenet equations:

$$\begin{aligned} \overrightarrow{T'} &= \vec{\omega} \times \vec{T} = \kappa\vec{B} \times \vec{T} &&= \kappa\vec{N} \\ \overrightarrow{N'} &= \vec{\omega} \times \vec{N} = \tau\vec{T} \times \vec{N} + \kappa\vec{B} \times \vec{N} &&= -\kappa\vec{T} + \tau\vec{B} \\ \overrightarrow{B'} &= \vec{\omega} \times \vec{B} = \tau\vec{T} \times \vec{B} &&= -\tau\vec{N} \end{aligned} \qquad \text{(A4.8)}$$

The above shows that torsion is an intrinsic characteristic of a 3 dimensional curve, it is not due to an additional rotator force. The latter is torque and will give rise to an additional rotation around the tangent. An elongated object of physical dimensions has a finite cross section. Folded in a 3 dimensional curve the cross section will rotate with a speed determined by the torsion. The change of its angle α (with respect to e.g. the beginning of the curve) as a function of travelled distance equals the torsion:

$$\frac{\partial \alpha}{\partial s} = \tau \qquad \text{(A4.9)}$$

A.5 Helix

In the forward calculations use is made of a helix curve. Here, we will give the formulas for the position, tangent vector, normal vector, binormal vector as well as curvature and torsion as function of the distance along the helix.

Position
$$\vec{r} = \begin{pmatrix} a\cos\left(\frac{s}{c}\right) \\ a\sin\left(\frac{s}{c}\right) \\ \frac{b}{c}s \end{pmatrix} \; with\; c = \sqrt{a^2 + b^2} \qquad \text{(A5.1)}$$

Tangent vector
$$\vec{T}(s) = \overrightarrow{r'}(s) = \begin{pmatrix} -\frac{a}{c}\sin\left(\frac{s}{c}\right) \\ \frac{a}{c}\cos\left(\frac{s}{c}\right) \\ \frac{b}{c} \end{pmatrix} \qquad \text{(A5.2)}$$

Normalization, Distance
$$\sqrt{\overrightarrow{r'}(s)\cdot\overrightarrow{r'}(s)} = 1 \;\rightarrow\; \int \sqrt{\overrightarrow{r'}(s)\cdot\overrightarrow{r'}(s)}\,ds = s \qquad \text{(A5.3)}$$

Curvature, Normal vector
$$\overrightarrow{r''}(s) = \frac{a}{c^2}\begin{pmatrix} -\cos\left(\frac{s}{c}\right) \\ -\sin\left(\frac{s}{c}\right) \\ 0 \end{pmatrix} = \kappa\vec{N}(s) \;\rightarrow\; \kappa = \frac{a}{c^2} \qquad \text{(A5.4)}$$

Binormal vector
$$\vec{B} = \vec{T}\times\vec{N} = \begin{pmatrix} \frac{b}{c}\sin\left(\frac{s}{c}\right) \\ -\frac{b}{c}\cos\left(\frac{s}{c}\right) \\ \frac{a}{c} \end{pmatrix} \qquad \text{(A5.5)}$$

Torsion
$$\overrightarrow{B'} = \frac{b}{c^2}\begin{pmatrix} \cos\left(\frac{s}{c}\right) \\ \sin\left(\frac{s}{c}\right) \\ 0 \end{pmatrix} = -\frac{b}{c^2}\vec{N} \;\rightarrow\; \tau = \frac{b}{c^2} \qquad \text{(A5.6)}$$

Both curvature and torsion are constant over the full curve. After 1 turn the distance travelled is $\Delta s = 2\pi c$, then the rotation of the cross section according (A4.9) equals $\Delta s.\tau = 2\pi b/c$. After 1 turn the vectors $\vec{T}, \vec{N}$ and $\vec{B}$ reproduce onto themselves. This means that any vector that is a linear combination of these vectors will also reproduce after 1 turn. However, the internal coordinate system of the physical cross section of the helix does turn, and will not return onto itself after a round trip. This explains why a spring with a helix shape is called a torsion spring.

A.6 Expanding helix

Similar to the previous paragraph we give here the formula's for an expanding helix, i.e. a helix of which the radius is constantly increasing. In this case the formulas will be given as a function of a parameter t not equalling the distance travelled.

Position
$$\vec{r}(t) = \begin{pmatrix} t\sin(t) \\ t\cos(t) \\ t \end{pmatrix} \tag{A6.1}$$

$$\vec{r'}(t) = \begin{pmatrix} \sin(t) + t\cos(t) \\ \cos(t) - t\sin(t) \\ t \end{pmatrix} \tag{A6.2}$$

Normalization
$$\left\|\vec{r'}(t)\right\| = \frac{ds}{dt} = \sqrt{2 + t^2} \tag{A6.3}$$

Distance
$$s(t) = \int \sqrt{2 + t^2}\, dt = \frac{t}{2}\sqrt{2 + t^2} + \ln\left[\frac{t + \sqrt{2 + t^2}}{\sqrt{2}}\right] \tag{A6.4}$$

Tangent
$$\vec{T}(t) = \frac{\vec{r'}(t)}{\left\|\vec{r'}(t)\right\|} = \frac{1}{\sqrt{t^2 + 2}}\begin{pmatrix} \sin(t) + t\cos(t) \\ \cos(t) - t\sin(t) \\ 1 \end{pmatrix} \tag{A6.5}$$

Normal
$$\vec{N}(t) = \frac{1}{\sqrt{t^2 + 2}\sqrt{t^4 + 5t^2 + 8}}\begin{pmatrix} -(3t + t^3)\sin(t) + (4 + t^2)\cos(t) \\ -(3t + t^3)\cos(t) - (4 + t^2)\sin(t) \\ -t \end{pmatrix} \tag{A6.6}$$

Curvature
$$\kappa(t) = \frac{\sqrt{t^4 + 5t^2 + 8}}{(t^2 + 2)^{3/2}} \tag{A6.7}$$

Binormal
$$\vec{B} = \vec{T} \times \vec{N} = \frac{1}{\sqrt{t^4 + 5t^2 + 8}}\begin{pmatrix} 2\sin(t) + t\cos(t) \\ 2\cos(t) - t\sin(t) \\ -2(2 + t^2) \end{pmatrix} \tag{A6.8}$$

Torsion
$$\tau(t) = -\frac{t^2 + 6}{t^4 + 5t^2 + 8} \tag{A6.9}$$